

Study of underpotential deposited Cu layers on Pt(111) and their stability against CO and CO₂ in perchloric acid

Cite this: *Phys. Chem. Chem. Phys.*, 2013, **15**, 19659

Christian Schlaup* and Sebastian Horch

The underpotential deposition (UPD) of copper on a Pt(111) electrode and the influence of gas coadsorbates, *i.e.* CO and CO₂, on the thus deposited copper layer were studied in a 0.1 M HClO₄ electrolyte by means of EC-STM. By UPD, an atomically flat Cu layer is formed, which exhibits a pseudomorphic (1 × 1) structure. However, it contains several point defects due to which its total coverage is less than a monolayer, in agreement with the measured charge density in the CV curves. Upon exposure to a CO-saturated solution the pseudomorphic structure collapses to a coalescent structure with many vacancy islands. This phase transition is induced by the preferential binding of CO to the Pt(111) surface. In contrast, CO₂, which binds stronger to copper, does not affect the pseudomorphic structure of the Cu layer.

Received 25th June 2013,
Accepted 3rd October 2013

DOI: 10.1039/c3cp52649f

www.rsc.org/pccp

1 Introduction

The electrochemical phenomenon that certain amounts of a metal can be deposited above the Nernst potential is known as underpotential deposition (UPD).¹ In contrast to bulk deposition at potentials below the Nernst potential, which is a continuous process, the UPD allows the deposition of metal adlayers with discrete and well defined coverages, generally covering the range of submonolayers to monolayers^{1,2} and for a few cases also multilayers, *e.g.* for silver on platinum.^{3,4}

The exact nature of these metal adlayers is not only determined by the involved metal species but also by the supporting electrolyte. Anions can coadsorb during the metal UPD and change the metal adlayer's structure and coverage. For example, even such a small concentration as 10⁻⁶ mol⁻¹ of Cl⁻ prevents the formation of a (2 × 2) phase during copper UPD on Au(111) electrodes.⁵ Also organic coadsorbates such as bis-(sodium-sulfopropyl)-disulfide (SPS) are known to influence the metal ad-/desorption and are used in industrial applications, such as the Damascene process.⁶ Coadsorbates can, however, not only affect the metal adlayer during the actual UPD, but also after deposition. This can be utilized, *e.g.*, to form ultrathin binary compound films by consecutive steps of metal UPD and exposure to reactive anions, known as EC-ALE.^{7,8}

In the present study, the response of an underpotential deposited copper adlayer on a Pt(111) surface to the adsorption of two complementary gasses, namely CO and CO₂, was studied by means of EC-STM. CO and CO₂ are complementary regarding

their binding preferences: whereas CO binds strongly to platinum surfaces⁹ and even suppresses Cu UPD when present during deposition,^{10,11} CO₂ binds stronger to copper.¹² Using these two gasses thus allows for investigating the response of the copper adlayer in the two opposite cases of preferential gas–substrate interactions and preferential gas–metal adlayer interactions. This might also be relevant for electrochemical CO₂ reduction, for which copper is the most active material and CO a key intermediate.^{13–17}

2 Experimental

STM and CV measurements were carried out in a custom-built EC-STM setup,¹⁸ using electrochemically etched Pt/Ir (90/10) tunneling tips with a hot-glue (PEVAC) coating. The tip potential is set and held constant during potentiodynamic imaging with respect to the working electrode, corresponding to a constant bias voltage but variable tip potential. For all measurements, a Pt wire serves as a pseudo-reference electrode, which has a fair stability in acidic electrolytes, having a potential accuracy of ±25 mV. However, due to the high affinity of platinum for CO, a significant potential shift upon introduction of CO into the system is observed. The consequences of this potential shift will be discussed in the corresponding section in detail. In order to provide comparability, all potentials are given with respect to the standard hydrogen electrode (SHE), unless otherwise noted.

A commercially available Pt(111) single crystal (MaTeck, Jülich) was prepared by flame annealing in a butane–air flame. After cooling down to room temperature in a high purity argon atmosphere (scientific grade, 99.9999%), it was protected with a droplet of ultrapure water and mounted into the electrochemical cell of the EC-STM.

Department of Physics, Technical University of Denmark, DK-2800 Kongens Lyngby, Denmark. E-mail: cgsc@fysik.dtu.dk



Electrolyte solutions were prepared using ultrapure water (Millipore, Milli-Q[®]), 70% HClO₄ (Merck, Suprapur[®]) and 99.9995% CuO (Alfa Aesar[®]). Before usage they were deaerated with argon (scientific grade, 99.9999%) and, if required, afterwards saturated with either CO (scientific grade, 99.997%) or CO₂ (scientific grade, 99.9992%).

In order to avoid tip induced artifacts, a freshly prepared STM tip was used for each measurement. For the measurements in the Cu-free electrolyte the tip was first mounted after the electrolyte exchange for a Cu-free solution.

3 Results and discussion

The first step was deposition of a copper film on the Pt(111) surface by underpotential deposition (UPD) from a 0.1 M HClO₄ + 1 mM CuO solution. This was followed by an electrolyte exchange for a *blank*, *i.e.* Cu-free, 0.1 M HClO₄ solution to remove all remaining Cu²⁺ cations from the liquid phase. Finally the Cu-modified Pt(111) electrode was subjected to either CO or CO₂ saturated 0.1 M HClO₄ solution by performing a second electrolyte exchange. In the following, each individual step will be characterized and discussed in detail.

3.1 Cu deposition on Pt(111)

For Cu deposition on the Pt(111) surface, the UPD from a 0.1 M HClO₄ + 1 mM CuO solution was utilized, which should lead to the formation of a pseudomorphic Cu monolayer.¹ Our CV curve of this particular system (gray curve in Fig. 1) is in good agreement with previous results.^{1,19,20} It exhibits two cathodic peaks at 690 mV and 540 mV, *i.e.* above the Nernst potential of 251 mV, which are generally assigned to the deposition of a Cu monolayer on the Pt(111) surface. For the subsequent anodic desorption a single sharp peak appears at a significantly higher potential of 730 mV. Both the significantly higher potential and the sharp peak shape reflect the quasi irreversible character of

this process, caused by attractive interactions between the adsorbed Cu atoms.²¹

The measured charge density of $(405 \pm 25) \mu\text{C cm}^{-2}$ for the Cu desorption is about 15% less than expected for a pseudomorphic Cu monolayer, assuming a transfer of 2 electrons per Cu atom ($480 \mu\text{C cm}^{-2}$). This lack of charge is known in the literature^{1,20} and denoted the coadsorption of anions during the Cu deposition. However, there is some disagreement concerning the charge value: whereas some ref. 1 and 20 report a value of $340 \mu\text{C cm}^{-2}$, a study of Marković *et al.*¹⁹ reports a dependence of the charge density on the Cu²⁺ concentration and quotes a value of $460 \mu\text{C cm}^{-2}$ for a 0.1 M HClO₄ solution containing 1 mM Cu²⁺, which is very close to the ideally expected value.

STM images recorded at potentials around 400 mV, *i.e.* after Cu deposition, show atomically smooth and homogeneous terraces (Fig. 2a). On high resolution images an atomic structure with hexagonal symmetry is found (Fig. 2b), which exhibits a nearest neighbor distance of $(2.77 \pm 0.04) \text{ nm}$. The atomic structure both fits with the lattice of the Pt(111) surface and is in good agreement with previous LEED results,^{1,22} which proposed a (1×1) structure for the Cu UPD phase. However, STM images also show some defects within the Cu layer (Fig. 2b), which actually indicates a lower Cu coverage. The defects' fraction of the Cu layer can be estimated at 0.1 ML, however, due to their random distribution and different sizes this should be just considered as a rough value. Also their origin remains unclear, even high resolution STM images do not reveal any specific adsorbate within these defects. In either case, they may explain most of the apparently missing desorption charge.

It should also be mentioned that the previous discussion²⁰ on the charge contribution of coadsorbed anions is based on a misinterpretation of the $(\sqrt{3} \times \sqrt{3})R30^\circ$ structure found for a Cu submonolayer on Au(111) electrodes. This structure was revealed in later studies^{1,2,23} to be formed by 0.33 ML of coadsorbed HSO₄⁻ anions stabilizing a $\Theta_{\text{Cu}} = 0.66 \text{ ML}$ Cu layer and not by a Cu layer with $\Theta_{\text{Cu}} = 0.33 \text{ ML}$.²⁰

Summarizing this discussion, it appears likely that underpotential deposition of copper on Pt(111) surfaces yields to the formation of a pseudomorphic overlayer with some local defects. They are also the reason for the apparent lack of desorption charge in the CV curves, with respect to an ideal, *i.e.* defect-free,

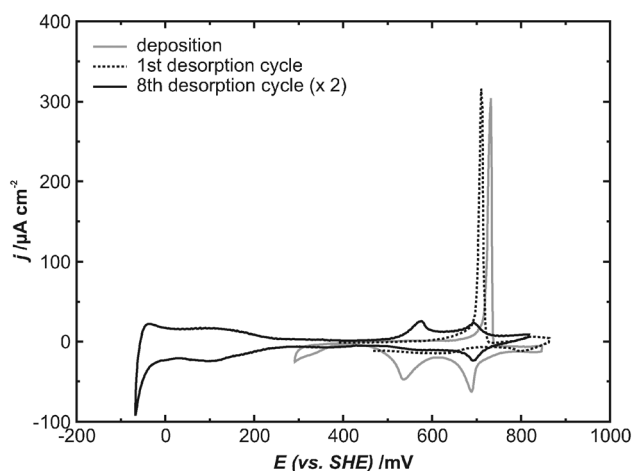


Fig. 1 Cyclic voltammograms of Cu-modified Pt(111), $dE/dt = 10 \text{ mV s}^{-1}$, gray line: the *deposition* electrolyte (0.1 M HClO₄ + 1 mM CuO), black lines: stripping of the Cu layer after exchange for the *blank* electrolyte (0.1 M HClO₄).

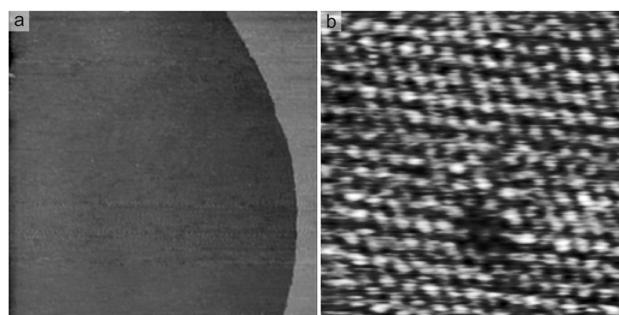


Fig. 2 STM images of the Cu-covered Pt(111) electrode in the *deposition* electrolyte (0.1 M HClO₄ + 1 mM CuO): (a) atomically flat morphology (552 nm^2), $E = 375 \text{ mV}$, $U_b = 156 \text{ mV}$, $I_T = 1 \text{ nA}$; (b) defective (1×1) -structure (4.63 nm^2), $E = 402 \text{ mV}$, $U_b = 1 \text{ mV}$, $I_T = 50 \text{ nA}$.



Cu-monolayer. However, the origin of these defects remains unclear, as STM images do not reveal any distinctive species within the defects. Based on these results, an actual Cu coverage of approximately 0.9 ML is assumed for the following, which forms a pseudomorphic (1×1)-structure on the Pt(111) surface.

3.2 Exchange for blank HClO₄ solution

The Cu deposition is followed by an electrolyte exchange for a *blank*, i.e. Cu-free, 0.1 M HClO₄ electrolyte, to prevent any further Cu deposition during the following experiments at lower potentials. This electrolyte exchange is carried out under potential control at a constant potential of 300 mV.

Cyclic voltammograms obtained in the blank electrolyte (black curves in Fig. 1) show that no copper is lost during the electrolyte exchange: in the first anodic scan a sharp desorption peak still appears, for which the same charge density as in the Cu²⁺ containing deposition electrolyte is measured (dotted curve in Fig. 1). During the following cycles only a fraction of the dissolved Cu²⁺ cations are redeposited during the cathodic scan, leading to a continuous shrinking of the desorption peak with the number of cycles due to the virtually infinite dilution of Cu²⁺ into the blank electrolyte. After several potential cycles, the CV curve shows the characteristic hydrogen-UPD and OH⁻ adsorption features for Pt(111) electrodes^{24,25} but only a very small Cu desorption peak (black curve in Fig. 1).

In order to minimize the risk of any Cu dissolution, the potential was decreased by 150 mV prior to the STM measurements. STM images recorded after the electrolyte exchange show that the Cu layer remains unchanged on the surface. Large scale images still exhibit an atomically smooth and homogenous morphology (Fig. 3a), which also proves that all Cu²⁺ cations are removed from the liquid phase and no Cu bulk deposition occurs. On high resolution images, a (1×1) structure with some fuzzy defects is found (Fig. 3b), showing that also the pseudomorphic structure of the Cu layer is retained.

3.3 Exposure of the Cu layer to CO

By performing a second electrolyte exchange for a CO-saturated 0.1 M HClO₄ solution, the Cu-modified Pt(111) surface was finally subjected to CO.

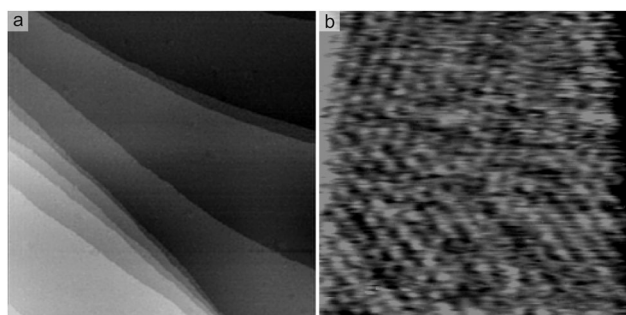


Fig. 3 STM images of the Cu-covered Pt(111) electrode after exchange for the *blank* electrolyte (0.1 M HClO₄): (a) atomically flat morphology (499 nm)², $E = 199$ mV, $U_B = 101$ mV, $I_T = 1$ nA; (b) (1×1)-structure with fuzzy defects (4.30 nm)², $E = 201$ mV, $U_B = 3$ mV, $I_T = 3$ nA.

3.3.1 Exchange for a CO-saturated solution. This electrolyte exchange was carried out at a constant potential of -650 mV with respect to the used pseudo-reference electrode. As already mentioned in the Experimental section, the reference potential is strongly influenced by CO. It decreases in the present case by about 450 mV, due to which the potential of the working electrode also drops by the same value (from initially +200 mV to -250 mV). As the resulting potential is significantly lower than the onset potential of the hydrogen evolution reaction (HER), the potential is increased after the electrolyte exchange to about -50 mV. During the whole procedure the Cu layer is only exposed to potentials which are lower than its deposition potential, due to which an anodic Cu desorption can be ruled out. However, it has to be considered whether the temporary exposure to strong HER has an effect on either its structure or morphology (Section 3.3.4).

3.3.2 Effect of CO on the Cu layer. The presence of CO in the electrolyte strongly affects the morphology of the Cu layer. Its initially flat and closed film like morphology collapses and many new vacancies are formed (Fig. 4a). Also diffusion of Cu into a second layer (Fig. 4b) or formation of cluster-like Cu accumulations is locally found (Fig. 5a). In either case, new vacancies within the Cu layer are formed, due to which part of the Pt(111) surface becomes directly exposed to the electrolyte and thus CO.

The rearrangement of the Cu layer is driven by the formation of attractive Pt–CO bindings. Their higher binding strength compared to Pt–Cu bindings is known from previous studies: in the presence of CO, the UPD of copper on Pt(100)¹¹ and Pt(111)¹⁰ electrodes vanishes. DFT calculations revealed a Pt(111)–CO binding energy of -1.5 eV, which is significantly more negative than the binding energy of CO to both, a pseudomorphic Cu layer on Pt(111) (-0.9 eV) and a pure

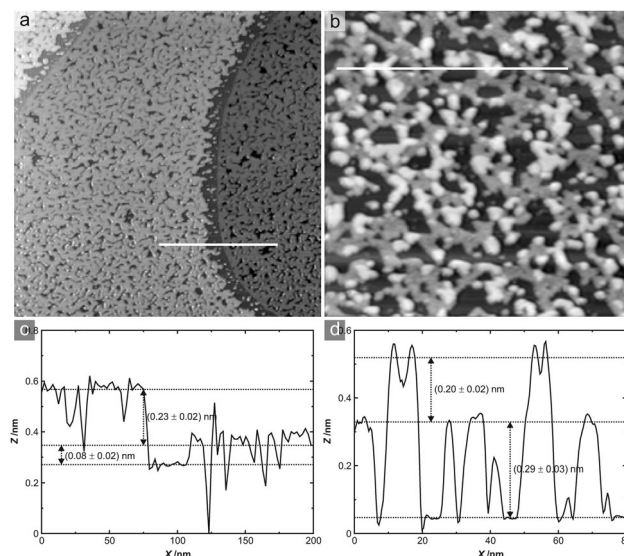


Fig. 4 Morphology of the Cu layer after exposure to CO: (a) coalescent defect structure (534 nm)², $E = -50$ mV, $U_B = 7$ mV, $I_T = 10$ nA; (b) partial diffusion into a 2nd Cu layer (108 nm)², $E = -42$ mV, $U_B = 100$ mV, $I_T = 1$ nA; (c) line profile to (a); (d) line profile to (b).



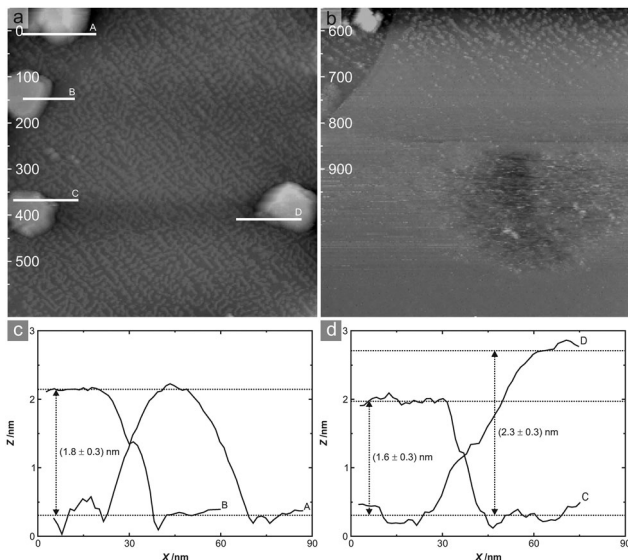


Fig. 5 Potentiodynamic STM images of the Cu dissolution in a CO-saturated 0.1 M HClO₄ electrolyte, the scale in the STM images corresponds to the potential in the current–voltage curve in Fig. 6: (a) (349 nm)², $E = -49$ mV to +547 mV, $U_B = 106$ mV, $I_T = 3$ nA; (b) (349 nm)², $E = 547$ mV to 936 mV, $U_B = 106$ mV, $I_T = 3$ nA; (c), (d) line profiles to (a).

Cu(111) surface (-0.6 eV).²⁶ Energetically it should thus be favorable to replace all copper by CO, which, however, is not possible because the Cu layer is stabilized by the low electrode potential against anodic dissolution. Consequently, one would expect that the copper agglomerates into large clusters in order to maximize the area of the Pt(111) surface making contact with CO.

However, no continuing morphology changes of the Cu layer towards cluster formation can be observed in the following STM images, indicating a suppression of Cu diffusion, both over the Pt(111) surface and into a second layer, in agreement with previous results that the adsorption of CO strongly influences the activation barriers for diffusion on platinum.²⁷ Hence, the newly formed defects do not originate from a long distance Cu mass transport, but from a local lateral compression of the initially pseudomorphic Cu layer to a more bulk-like structure. The diffusion into a second or a higher layer is only possible in the initial stage of the electrolyte exchange for the CO-saturated solution, while the CO concentration at the surface is still gradually increasing due to the limited flow-rate. Once the saturation concentration is reached (about 1–2 seconds) all further diffusion is suppressed. Consequently no evidence of an ongoing Cu diffusion can be found in STM images, such as a change in the Cu step edges to a more equilibrium shape or a growth of higher Cu islands.

Line profiles of the coalescent Cu islands exhibit a relative height of about 0.3 nm with respect to the CO-covered Pt(111) surface (Fig. 4c and d). This is significantly higher than for a pseudomorphic Cu film, for which one would expect a relative height of about 0.21 nm. Moreover, they appear even higher than the steps of the Pt(111) substrate (Fig. 4c). On the one hand this is due to the lateral compression of the Cu layer

during CO adsorption, forcing Cu atoms to less ideal adsorption sites, e.g. on-top sites. On the other hand different materials exhibit different local densities of states due to which their relative height in STM images does not necessarily reflect the topological height difference. This may get even more pronounced in the presence of adsorbates, in particular in the case of different binding properties. However, for the second Cu layer a relative height of about 0.2 nm can be measured (Fig. 4d), which is within the expected range of Cu step heights, such as 0.21 nm for Cu(111) and 0.18 nm for Cu(100).

One of the rare cases of larger cluster-like Cu accumulations is shown in Fig. 5a. The Cu coverage in the vicinity of the clusters is reduced to about 0.6 ML. The clusters have a height of about 1.6 nm to 2.3 nm (Fig. 5c and d), roughly corresponding to 8 to 11 Cu layers. The total amount of copper in these clusters can thus be estimated at 0.6 ML in this image. Both the existence of the clusters and the locally different Cu coverage indicate that Cu diffusion has locally been possible during the electrolyte exchange. As these clusters are very rare, the reason for this locally enhanced diffusivity remains unclear.

3.3.3 Cu dissolution in the presence of CO. The presence of CO also has a strong influence on the anodic Cu desorption, which is studied by consecutively recorded STM images while simultaneously increasing the electrode potential with a linear ramp of 10 mV s⁻¹. The y-axis of such *potentiodynamic* STM images (Fig. 5a and b) is thus directly correlated to the potential axis of the simultaneously recorded current–voltage curve (Fig. 6).

These images reveal that the coalescent Cu layer remains unchanged up to a potential of about 550 mV (Fig. 5a). However, during the further potential increase to about 700 mV, it disappears completely from the Pt(111) surface (Fig. 5b). In contrast to the desorption in a CO-free solution (Fig. 1), the simultaneously recorded current–voltage curve does not show a

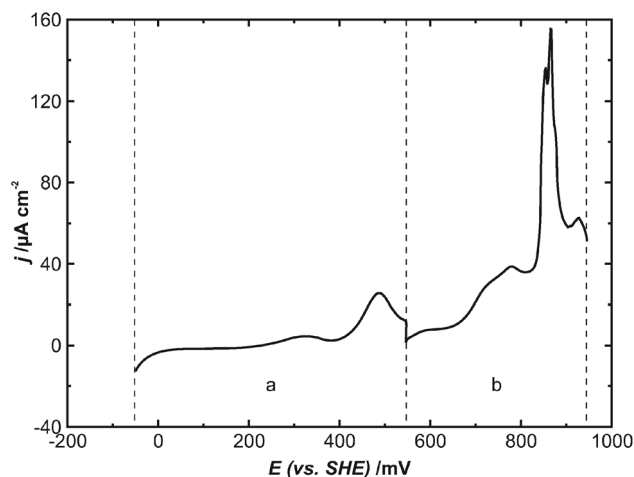


Fig. 6 Current–voltage curve from -49 mV to +936 mV recorded simultaneously with STM images in Fig. 5, after which the potential was kept constant, $dE/dt = 10$ mV s⁻¹, dashed lines: corresponding sections to the STM images (a/b), potential was kept constant in-between the images.



sharp current spike in this particular potential range, which would indicate an oxidation of the Cu layer and thus explain directly its disappearance in the STM image (Fig. 6). It only shows a rather broad current wave at a potential of about 500 mV, where, however, the Cu layer remains unchanged in the STM image (Fig. 5a). Also the total anodic charge density during the potential increase to 700 mV, which can be estimated at $(220 \pm 50) \mu\text{C cm}^{-2}$, is significantly lower than that measured for the anodic desorption of the Cu layer in an Ar-saturated solution. Only upon further potential increase can a prominent current peak be observed at a potential of about 850 mV. This peak, however, is known in the literature for the oxidation of adsorbed CO on the Pt(111) surface.^{28,29} Moreover, the overall shape of the current–voltage curve, including the peaks at 500 mV and 750 mV, is in good agreement with that for a completely Cu-free system, i.e. a Pt(111) electrode in a CO-saturated 0.1 M HClO₄ electrolyte.²⁹

Accordingly, no feature in the current–voltage curve can be directly correlated with the oxidation and thus disappearance of the Cu film in STM-images, even though, for desorption, it has to be oxidized. However, it might be possible that either adsorption of CO on the previously Cu-covered regions of the Pt(111) electrode or the onset of bulk CO oxidation screens the charge transfer for the anodic Cu dissolution.

Also in the STM images the exact potential for the Cu desorption remains ambiguous. Although the Cu layer seems to disappear at a potential of about 700 mV, it may not necessarily desorb into the electrolyte. Alternatively the onset of the oxidation of CO, which stabilizes the coalescent structure of the Cu layer, might lower the barrier for Cu diffusion and thus trigger a phase transition to a mobile phase. Such a mobile phase may appear invisible for STM, yielding in atomically flat and apparently adsorbate free terraces. Thus it remains unclear whether the apparently adsorbate free terraces in the potential range between 700 mV and 850 mV (Fig. 5b) indicate Cu desorption. The only notable additional feature is a fuzzy depression suddenly appearing at a potential of about 850 mV (Fig. 5b). This feature is coincident with the CO oxidation peak in the current–voltage curve (Fig. 6). Thus it may correspond to some disturbances of the STM caused by the CO oxidation, or alternatively, it may also indicate the desorption of a mobile Cu-adlayer into the electrolyte.

In summary, both Cu desorption and CO oxidation cannot be considered as isolated processes; they appear rather related to each other and occur under very similar potential conditions. Even though STM images suggest a desorption potential of about 650 mV, it remains unclear whether it corresponds to an alternative transition to a mobile phase.

3.3.4 Influence of HER. In order to prove that the morphology changes of the Cu layer described in Section 3.3 are purely CO-induced, the Cu layer was also subjected to strong HER in a CO-free 0.1 M HClO₄ electrolyte. By decreasing the potential to about -240 mV, at which a current density for HER of about $-600 \mu\text{A cm}^{-2}$ is reached, similar conditions to those to which the Cu layer was exposed during the electrolyte exchange for the CO saturated solution were modeled. After increasing the

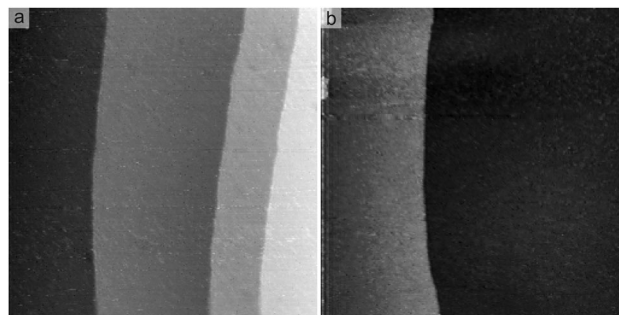


Fig. 7 (a) Atomically flat morphology of the Cu film after exposure to: (a) strong HER in Ar-saturated solution (517 nm^2), $E = 350$ mV, $U_B = 12$ mV, $I_T = 20$ nA; (b) a CO₂-saturated electrolyte (513 nm^2), $E = 208$ mV, $U_B = 103$ mV, $I_T = 10$ nA.

potential to about 300 mV, STM measurements were carried out, which show that strong HER has no influence on the morphology of the Cu film. STM images clearly show that the Cu layer retains its atomically smooth morphology (Fig. 7a) and no transition to a coalescent structure as in the CO saturated solution can be found. This supports the previous discussion of a purely CO-induced coalescence of the Cu film.

3.4 Exposure to a CO₂ saturated solution

For CO₂ an inverse binding situation with respect to CO can be assumed. Hence a morphology change of the Cu layer would be induced by Cu–CO₂ rather than Pt–CO₂ bindings.

To investigate this situation, a second electrolyte exchange for a CO₂-saturated 0.1 M HClO₄ electrolyte was performed after preparation of the Cu layer. STM images recorded at a potential of about 200 mV exhibit that the morphology of the Cu film remains unchanged and atomically smooth (Fig. 7b). Hence, the Cu film is stabilized by the Pt(111) surface against CO₂-induced morphological changes. Also, in agreement with the literature,³⁰ no restructuring induced by attractive Pt–CO₂ bindings can be found, in contrast to the results in a CO-saturated electrolyte. However, it has to be considered that copper is generally able to reduce CO₂ to CO,^{13,14,16,17} which may eventually lead to the same morphology changes as is observed in a CO-saturated solution.

4 Conclusions

The UPD of copper on a Pt(111) electrode and the influence of CO and CO₂ coadsorbates on the thus deposited Cu films have been studied by means of EC-STM. UPD leads to the formation of a Cu layer with a pseudomorphic (1 × 1) structure, in agreement with previous LEED studies. However, the Cu layer also contains some point defects, which naturally cannot be observed with LEED. Even though their origin remains unclear in STM images, they suggest an alternative understanding of the known, too low charge transfer during the Cu deposition: instead of a charge contribution from coadsorbed anions, the total Cu coverage is reduced by these defects.

Exposure to CO leads to a rearrangement of the Cu layer from its initially pseudomorphic structure to a defective coalescent



structure, which is driven by the formation of attractive Pt–CO bindings. CO also influences the anodic Cu dissolution: while the Cu layer apparently disappears in STM at a potential of about 650 mV, the simultaneously recorded current–voltage curve does not indicate any related anodic current and has virtually the same appearance as for a completely Cu-free system.

In contrast, exposure to CO₂, which should bind more attractive to copper rather than platinum, does not yield rearrangement of the Cu layer. Obviously its binding to the Pt(111) surface stabilizes it against a CO₂-induced restructuring. However, as CO₂ may get reduced to CO over copper, a CO-induced restructuring of the Cu layer may occur after longer exposures.

Acknowledgements

The Danish National Research Foundations Center for Individual Nanoparticle Functionality (DNRF54) is gratefully acknowledged for funding.

References

- 1 E. Herrero, L. Buller and H. Abruna, *Chem. Rev.*, 2001, **101**, 1897–1930.
- 2 M. F. Toney, J. N. Howard, J. Richer, G. L. Borges, J. G. Gordon, O. R. Melroy, D. Yee and L. B. Sorensen, *Phys. Rev. Lett.*, 1995, **75**, 4472–4475.
- 3 N. Kimizuka and K. Itaya, *Faraday Discuss.*, 1992, **94**, 117–126.
- 4 N. S. Marinkovic, J. X. Wang, J. S. Marinkovic and R. R. Adzic, *J. Phys. Chem. B*, 1998, **103**, 139–144.
- 5 J. Hotlos, O. Magnussen and R. Behm, *Surf. Sci.*, 1995, **335**, 129–144.
- 6 N. Hai, T. Huynh, A. Fluegel, M. Arnold, D. Mayer, W. Reckien, T. Bredow and P. Broekmann, *Electrochim. Acta*, 2012, **70**, 286–295.
- 7 T. L. Wade, R. Vaidyanathan, U. Happek and J. L. Stickney, *J. Electroanal. Chem.*, 2001, **500**, 322.
- 8 K. Varazo, M. D. Lay, T. A. Sorenson and J. L. Stickney, *J. Electroanal. Chem.*, 2002, **522**, 104.
- 9 S. Kelemen, T. Fischer and J. Schwarz, *Surf. Sci.*, 1979, **81**, 440–450.
- 10 C. Lucas, N. Marković and P. Ross, *Surf. Sci.*, 2000, **448**, 77–86.
- 11 C. Lucas, N. Marković, B. Grgur and P. Ross, *Surf. Sci.*, 2000, **448**, 65–76.
- 12 N. Schumacher, K. Andersson, L. Grabow, M. Mavrikakis, J. Nerlov and I. Chorkendorff, *Surf. Sci.*, 2008, **602**, 702–711.
- 13 Y. Hori, A. Murata, R. Takahashi and S. Suzuki, *J. Am. Chem. Soc.*, 1987, **109**, 5022–5023.
- 14 Y. Hori, R. Takahashi, Y. Yoshinami and A. Murata, *J. Phys. Chem. B*, 1997, **101**, 7075–7081.
- 15 Y. Hori, *Modern Aspects of Electrochemistry*, Springer, New York, 2008, pp. 89–189.
- 16 A. A. Peterson, F. Abild-Pedersen, F. Studt, J. Rossmeisl and J. K. Nørskov, *Energy Environ. Sci.*, 2010, **3**, 1311–1315.
- 17 W. Durand, A. Peterson, F. Studt, F. Abild-Pedersen and J. Nørskov, *Surf. Sci.*, 2011, **605**, 1354–1359.
- 18 M. Wilms, M. Krufft, G. Bermes and K. Wandelt, *Rev. Sci. Instrum.*, 1999, **70**, 3641–3650.
- 19 N. Marković and P. Ross, *Langmuir*, 1993, **9**, 580–590.
- 20 L.-W. Leung, T. Gregg and D. Wayne Goodman, *Chem. Phys. Lett.*, 1992, **188**, 467–470.
- 21 J. Greeley, *Electrochim. Acta*, 2010, **55**, 5545–5550.
- 22 L.-W. Leung, T. Gregg and D. Wayne Goodman, *Langmuir*, 1991, **7**, 3205–3210.
- 23 M. Nakamura, O. Endo, T. Ohta, M. Ito and Y. Yoda, *Surf. Sci.*, 2002, **514**, 227–233.
- 24 A. Berná, V. Climent and J. Feliu, *Electrochem. Commun.*, 2007, **9**, 2789–2794.
- 25 A. Hitotsuyanagi, M. Nakamura and N. Hoshi, *Electrochim. Acta*, 2012, **82**, 512–516.
- 26 M. Mavrikakis, B. Hammer and J. Nørskov, *Phys. Rev. Lett.*, 1998, **81**, 2819–2822.
- 27 M. Kalff, G. Comsa and T. Michely, *Phys. Rev. Lett.*, 1998, **81**, 1255–1258.
- 28 N. Marković, B. Grgur, C. Lucas and P. Ross, *J. Phys. Chem. B*, 1999, **103**, 487–495.
- 29 J. Inukai, D. A. Tryk, T. Abe, M. Wakisaka, H. Uchida and M. Watanabe, *J. Am. Chem. Soc.*, 2013, **135**, 1476–1490.
- 30 N. Hoshi and Y. Hori, *Electrochim. Acta*, 2000, **45**, 4263–4270.

